Article

Journal of the Brazilian Chemical Society

https://dx.doi.org/10.21577/0103-5053.20240164

J. Braz. Chem. Soc. **2024**, *35*, 12, e-20240164, 1-13

Influence of Graphene Oxide Concentration and Fluorophore Charge on the Formation of Non-Fluorescent GO-Fluorophore Complexes

Danilo R. C. Ferreira,[a] Tiago Serodre,[a,b] Pedro L. Gastelois,[a] Waldemar A. A. Macedo,[a] Estefânia M. N. Martins[a] and Clascídia A. Furtado[*,a]*

[a]*Centro de Desenvolvimento da Tecnologia Nuclear (CDTN), 31270-901 Belo Horizonte-MG, Brazil*

[b]*Laboratoire Charles Coulomb, L2C, Université de Montpellier/CNRS, 34095 Montpellier, France*

The Stern-Volmer equation is commonly used to describe the fluorescence quenching process, but its application faces challenges for quenchers with heterogeneous physicochemical characteristics (size and surface composition), such as graphene oxide. This study proposes a mathematical approach to calculate the association constant and the change in the Gibbs free energy in graphene oxide-fluorophore systems, considering the influence of quencher concentration (0.12 to 250 μg mL^{-1}) and the net charge of the fluorophore on the formation of the non-fluorescent complex. It was identified that increasing the concentration of graphene oxide favors the formation of the non-fluorescent complex in the interaction with charged fluorophores, starting from 0.48 μg mL^{-1} for methylene blue and from 31.25 μg mL^{-1} for fluorescein sodium, predominantly leading to static fluorescence quenching. The interaction between graphene oxide and naphthalene lead to dynamic fluorescence quenching. This evaluation could be explored, for example, in nanotechnologies for environmental and biomedical applications.

Keywords: fluorescence quenching, Stern-Volmer equation, graphene oxide, fluorescein sodium, methylene blue, naphthalene

Introduction

Fluorescence is the phenomenon that occurs when a fluorophore absorbs an exciting photon, raising an electron to an excited energy state, with the subsequent relaxation of the electron to its ground state by emitting a photon of longer wavelength. This phenomenon can be disrupted by a process known as quenching, in which the photon emission is deactivated due to the external action of a quencher. Quenching can occur via two mechanisms: static, involving the formation of a non-fluorescent complex, or dynamic, through resonant energy transfer.[1] In quencher-fluorophore pair systems, both quenching mechanisms may occur simultaneously, with one usually being more predominant than the other. The quenching process can be exploited in the structural study of proteins,[2-4] membranes,[5,6] in microscopy analyses,[7,8] environmental analyses,[9,10] and, more recently, in detection mechanisms in biosensor systems.[11-14] These last two, taking advantage of the promising use of the fluorescence quenching phenomenon in the construction of sensitive and specific sensors, whether for gases, pollutants, or biomarkers such as cancer, bacteria, and viruses.

The quenching process is commonly described by the Stern-Volmer equation and its variants, which can be used to calculate the values of the association constant (K_{as}) and the Gibbs free energy of association (ΔG_{as}) of the quencher-fluorophore pair. However, the parameters obtained by this methodology represent only an average of the process as a whole. Since quenching process is highly sensitive to the characteristics of the medium and the concentration of the reagents, varying significantly as these conditions are modified,[1] the Stern-Volmer equation and its variants, which are based on the molar concentration of the reagents, face significant challenges in systems using quenchers with heterogeneous physicochemical characteristics. This is because when a nanoparticle or nanomaterial has its size described by a distribution curve and its functionalization pattern and degree are variable, the definition of molarity becomes unclear. A quencher that exhibits this behavior and shows promising technological applicability is graphene oxide (GO).[15,16]

*e-mail: clas@cdtn.br
Editor handled this article: Aldo José Gorgatti Zarbin (Guest)
"In honor of Prof Oswaldo Luiz Alves, for all the teachings, encouragement, support, and inspiration, and for being a great example to the Brazilian scientific community."

GO is a two-dimensional nanometric carbonaceous structure that possesses remarkable physicochemical properties, such as water dispersibility,[17] large specific surface area,[18] and excellent fluorescence quenching capacity.[15,16] The high quenching capacity of GO has been extensively studied for the construction of biosensors.[19-22]

In this context, the present study is based on GO-fluorophore systems to propose a mathematical model capable of approximating point-by-point the values of K_{as} from a quenching efficiency curve as a function of quencher concentration. Additionally, the influence of the fluorophore net charge in favoring the formation of the non-fluorescent complex was evaluated.

Results and Discussion

Characterization of the synthesized graphite oxide (GrO) and graphene oxide (GO)

The physicochemical characterization of the GrO and GO is illustrated in Figure 1. X-ray diffraction (XDR) and Raman spectroscopy of graphite oxide (GrO) characterize the conversion of ground expanded graphite into graphite oxide.[23,24] Figure 1a shows the obtained diffractogram, with a peak around 10° associated with the reflection of the (002) plane of graphite oxide. There is no peak at 26.5°, corresponding to the reflection of the (002) plane of graphite.[24-27] Using Bragg's law, a distance of 8.0 Å between the planes of GrO was calculated. The increase in distance between the planes of GrO compared to the interplanar distance of 3.4 Å of graphite is caused by steric and charge repulsion effects of the oxygenated groups added to the surface of these planes, resulting in the weakening of π-π interactions.

The Figure 1a insert shows characteristic Raman bands of graphite structures: the G band, centered at 1582 cm^{-1}, associated with the stretching of C=C bonds in the hexagonal network in regions of order and integrity of the crystalline structure, and the D band, centered at 1353 cm^{-1}, related to the breathing mode of the carbon ring, activated by the presence of defects in the hexagonal graphene network.[23,26-31] The ratio between the D and G bands (I_D/I_G) of around 0.9 indicates the presence of defects likely related to the addition of oxygenated groups in the graphitic network. Recent studies[32-34] indicate that the I_D/I_G ratio does not increase steadily with the degree of oxidation, and, therefore, it should not be used to quantify the degree of oxidation of the nanostructure. For the identification and quantification of oxygenated groups, the GrO sample was characterized by attenuated total reflectance-Fourier transform infrared spectroscopy (ATR-FTIR), X-ray photoelectron spectroscopy (XPS) and potentiometric titration.

In the ATR-FTIR analysis (Figure 1b) bands corresponding to the following vibrations can be identified: the stretching of the –OH bond of alcohols and phenolic groups (3400 cm^{-1}), the stretching of the –OH bond of carboxylic groups (3230 cm^{-1}), the stretching of C=O bonds (1720 cm^{-1}), the stretching of C=C bonds (1625 cm^{-1}), the stretching of the C–O bonds of phenols (1427 cm^{-1}), and the stretching of the C–O bonds of epoxy groups (1010 cm^{-1}), in agreement with the literature results for GrO and GO.[35-37]

The elemental composition of sample GrO was determined from the analysis of the survey XPS spectrum shown in Figure 1c. The elemental composition of sample GrO was found to be 68.0% carbon, 30.3% oxygen (C/O ratio about 2.3) and 0.9% sodium, with traces of iron and sulfur. The high-resolution spectrum in the region of the C 1s peak (insert of Figure 1c) reveals an intense peak around 284.5 eV, corresponding to the C–C bonds in the graphitic basal plane of the GrO sample.[38,39] At higher energies, contributions attributed to oxygenated groups are present, which can be deconvoluted into two peaks. One is centered around 287.0 eV, corresponding to epoxy, hydroxyls, and phenolic groups, while the other is centered around 289.5 eV, corresponding to lactones and carboxyls,[38,39] corroborating with the FTIR analysis.

By potentiometric titration, the functional groups present in the GO sample exhibited pK_a values that can be associated with carboxylic acid groups (pK_a 4.0, and 5.8), lactones (pK_a 7.0), and phenols (pK_a 8.8, and 9.7),[39-41] frequently observed in GrO and GO samples produced by similar methodologies.[39,42] The quantities of each functional group were 0.73 mmol g^{-1} of carboxylic acid, 0.31 mmol g^{-1} of lactones, and 1.15 mmol g^{-1} of phenols, indicating a prevalence of –OH groups on the nanostructure surface.

Once the conversion of graphite into graphite oxide (GrO) was confirmed, a dispersion of graphene oxide (GO) was produced as described in the Experimental section (insert of Figure 1e). Figure 1d shows an atomic force microscopy (AFM) image of the sample, where the shape and distribution of thickness, and mainly the size of the GO sheets present in the dispersion can be illustrated. The lateral size of the sheets varies between approximately 0.5 and 3 μm, with a predominance of smaller lateral size sheets and thickness around 2 nm, which corresponds to the thickness of two or fewer layers of graphene oxide.[43] The histogram constructed from the statistical analysis of 6000 flakes (Figure 1e) shows the distribution of topographic area of the GO sheets ranging from 1×10^{-4} μm^2 to greater than 1 μm^2, with a prevalence of 64% of the sheets with an

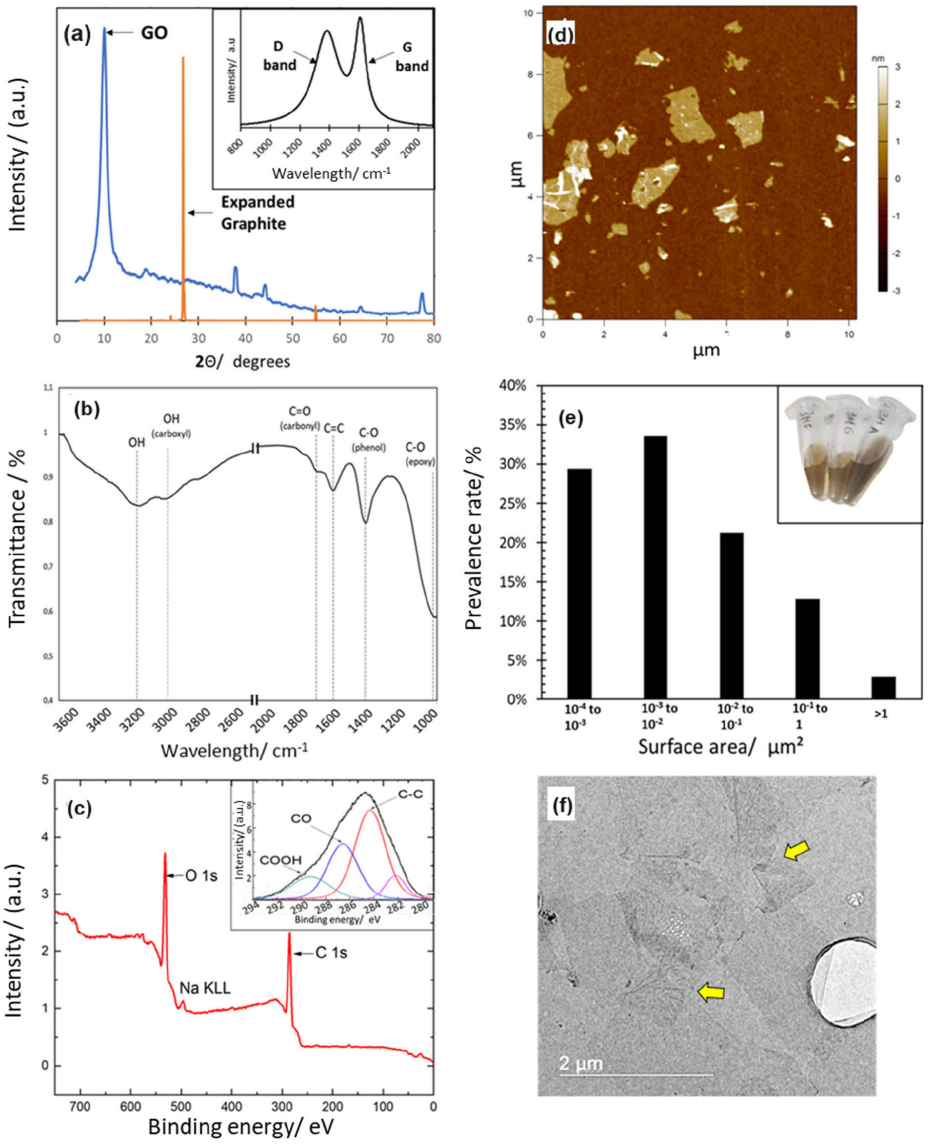

Figure 1. Physicochemical and morphological characterization of synthesized graphite oxide (GrO) and graphene oxide (GO). (a) X-ray diffraction of GrO with Raman spectroscopy in the insert showing typical GrO pattern; (b) attenuated total reflectance-Fourier transform infrared spectroscopy (ATR-FTIR) spectra of GrO; (c) elemental composition of GrO from survey monochromatic X-ray photoelectron spectroscopy (XPS) with high-resolution XPS in the insert; (d) atomic force microscopy (AFM) images of GO sheets, showing their typical morphology; (e) topographic area distribution of GO sheets determined by AFM with GO dispersions in water shown in the insert; (f) transmission electron microscopy (TEM) image of GO sheets after exfoliation in water.

area smaller or equal to 1×10^{-2} µm^2. From the transmission electron microscopy images, it is also possible to observe that sheets with larger area show regions where the 2D sheet folds onto itself (yellow arrows Figure 1f). This flexibility is not observed in intact graphite sheets, consisting only of sp^2 carbons but rather in nanostructures with a high degree of functionalization, such as GO.[44]

Given the physicochemical characteristics exhibited by GrO and GO (Figures 1a-1e), which demonstrate their heterogeneity in size and surface composition, it can be understood that the dispersion of GO belongs to the group of dispersions that do not have a clear definition of a basic unit capable of exhibiting all the characteristics of the system and representing its entirety. Consequently, the definition of the unit cell of the crystal and the molarity of GrO and GO becomes imprecise. The representation of the GO surface itself is subject to study, with various representations being considered.[45-49]

GO as fluorescence quencher

The ability of the GO (0 to 250 µg mL^{-1}) to quench the fluorescence was investigated for three fluorophores with different net charges: fluorescein sodium (FS), which has a negative net charge; naphthalene (NP), which is neutral; and methylene blue (MB), which has positive net charge.

The Stern-Vomer curves of the fluorescence quenching caused by GO for these three fluorophores are shown in Figure 2.

The Stern-Volmer curve (equation 1) establishes a linear relationship between the concentration of the quencher [Q] and the quotient of the fluorescence intensity in the absence of the quencher (F_0) by the fluorescence intensity in its presence (F_q):

$$\frac{F_0}{F_q} = 1 + K_{SV}[Q] \quad (1)$$

It is important to emphasize that before applying equation 1, it is necessary to correct the observed fluorescence intensity values for the inner filter effect, since the GO dispersions are very optically dense, exceeding 10% absorption for certain concentrations.[50] The correction is given by equation 2, where F_{cor} and F_{obs} are the corrected and observed fluorescence intensities, respectively, and Ab_{exc} and Ab_{em} are the absorbance of the system at the excitation and emission wavelengths of the fluorophore, respectively:

$$F_{cor} = F_{obs} \times 10^{\frac{Ab_{exc}+Ab_{em}}{2}} \quad (2)$$

Figures 2d and 2e shows that for all GO-fluorophore pairs at concentrations of 100 and 10 nmol L^{-1}, the interaction can be well described by equation 1, except for the GO-MB pair at 100 nmol L^{-1}. In this case, a curve with

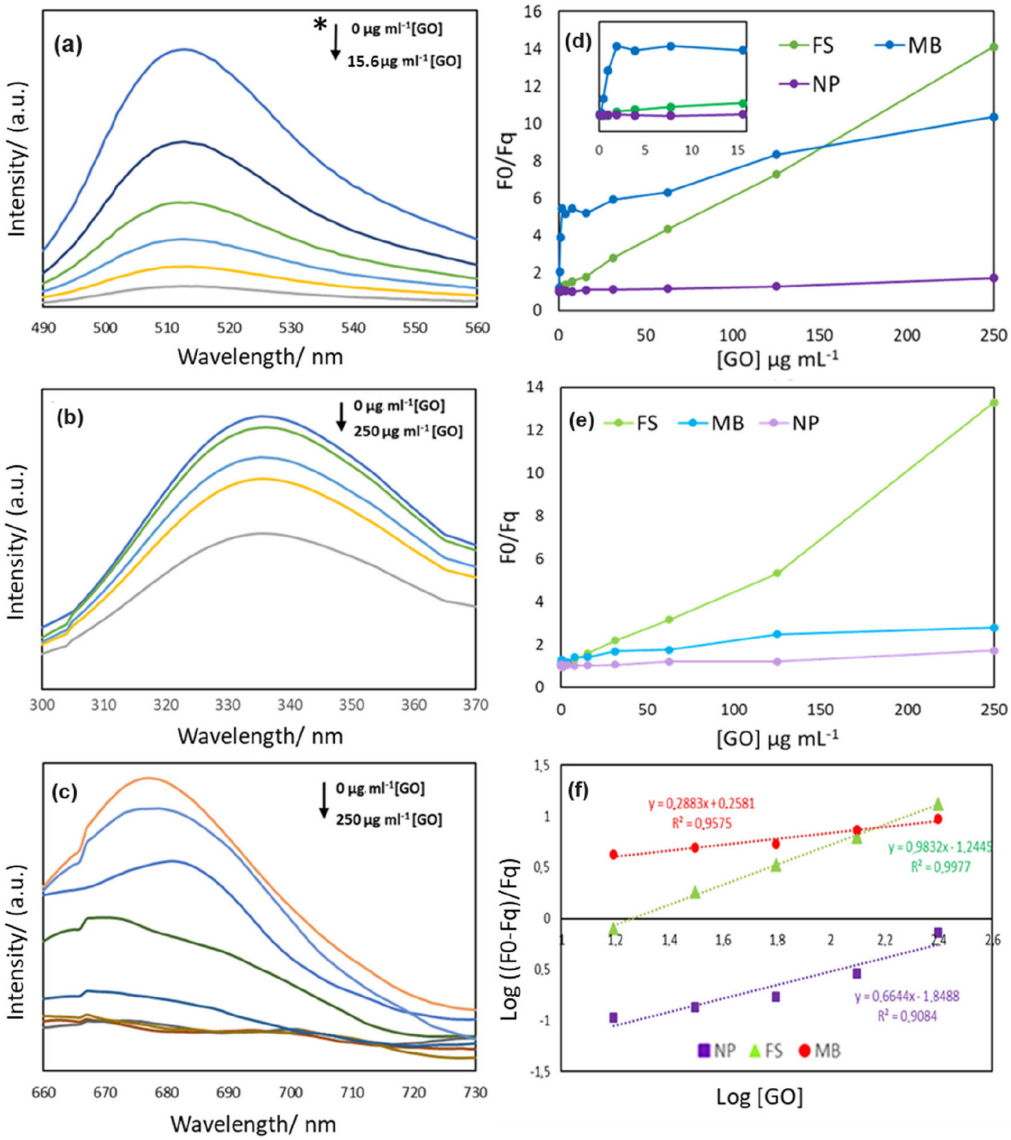

Figure 2. Fluorescence spectrum in the increasing presence of GO for (a) fluorescein sodium (FS), (b) naphthalene (NP), and (c) methylene blue (MB). Stern-Volmer curves of FS, NP, and MB at concentrations of (d) 100 nmol L^{-1}; (e) 10 nmol L^{-1}; and (f) modified Stern-Volmer curves for NP, FS, and MB at a concentration of 100 nmol L^{-1}. *Due to the high quantum yield of the FS, it was chosen to display the graph only for the lower concentrations so that the fluorescence quenching pattern could be better visualized.

a logarithmic shape was observed, where there is a rapid increase in the value of F_0/F_q, followed by the formation of a plateau (insert of Figure 2d). This behavior is similar to the adsorption saturation curves of MB on GO samples.[51-54] The value of F_0/F_q for the GO-MB pair at 100 nmol L^{-1} increases up to 5 times compared to the other GO-fluorophore pairs.

Another important point to emphasize is that the Stern-Volmer equation (equantion 1) assumes that the quencher concentration is in units of molarity. However, particularly in the case of nanomaterials, authors of fluorescence quenching studies[15,16,19-22] often use mass concentration when applying the Stern-Volmer plot. This strategy is necessary because defining the molarity of a nanoparticle or nanomaterial can be difficult and imprecise. This limitation should be acknowledged in the studies, as the direct correlation between mass and molarity may not be 1:1, leading to deviations in the Stern-Volmer plot.

Another deviation from the linearity of the Stern-Volmer curve (equation 1) can occur in systems that simultaneously exhibit static and dynamic quenching mechanisms. As it is not possible to distinguish and specify the occurrence of one or the other type of quenching solely by applying the Stern-Volmer equation, other mathematical models, such as the Lineweaver-Burk[55,56] model and the modified Stern-Volmer curve (Figure 2f), have been used as alternatives.[1,55,56]

The modified Stern-Volmer curve establishes a relationship between the logarithm of the ratio of the fluorescence intensity that did not undergo quenching ($F_0 - F_q$) and the fluorescence intensity that did undergo quenching (F_q), and the logarithm of the quencher concentration ([GO]).

$$\log\left(\frac{F_0 - F_q}{F_q}\right) = \log K_{as} + n \times \log[GO] \quad (3)$$

$$\Delta G_{as} = -RT\ln K_{as} \quad (4)$$

With equation 3, it is possible to calculate the value of the association constant (K_{as}) by taking the antilogarithm of the invariant term of this linear equation, resulting in a value of 1.4×10^{-3} for NP, 5.7×10^{-2} for FS, and 1.8 for MB. Using the calculated values of K_{as} in the Gibbs free energy equation (equation 4), it is possible to estimate how favorable the formation reaction of the non-fluorescent complex (static quenching) is. Assigning the value of the universal gas constant R (8.3145 J mol^{-1} K^{-1}) and the absolute temperature T (in this case, 298 K), the Gibbs energy was calculated, resulting in 4.58 kJ mol^{-1} for NP, 3.08 kJ mol^{-1} for FS, and –0.64 kJ mol^{-1} for MB. These values indicate that the occurrence of the static quenching mechanism in the GO-NP and GO-FS pairs is unfavorable, while it is favorable in the GO-MB pair.

The value of K_{as} provided by equation 3 indicates the thermodynamics of the process as a whole. However, it is possible for a change in the predominance of one type of quenching to occur when one of the reactants is increased. The static quenching mechanism may be favored by increasing the concentration of either the quencher or the fluorophore since in a short-range interaction (such as a chemical reaction or hydrogen bonding), the equation for the formation of the non-fluorescent complex can be shifted towards the formation of the product. Thus, the use of equation 3 to estimate the value of K_{as} has been suggested only in specific cases where the molar ratio of fluorophore to quencher is known to be 1:1, their stoichiometric coefficients are equal to 1, and the interaction of one site does not compete with another.[57] Furthermore, in cases of quencher dispersions with heterogeneous characteristics (such as particle size distribution, spatial position of functional groups, and numbers of layers), such as GO, the imprecision in defining molarity prevents the proper use of equation 3 for estimating K_{as}. Additionally, the size distribution and heterogeneity of the position of functional groups make the physicochemical properties of each sheet different from each other. It is possible, for example, that two sheets with the same surface area exhibit completely different quenching capacities, as quenching in graphene and its derivatives is directly related to the integrity of the hexagonal carbon network. As described by Morales-Narváe and Merkoçi,[15,18] the quenching capacity of graphene is inversely proportional to the degree of oxidation and directly proportional to the lateral size of the sheet.

Thus, this study proposes a new methodology to estimate the values of K_{as} and infer about the fluorescence quenching mechanism when using GO dispersions as quenchers.

As it involves a strong and short-range interaction, the non-fluorescent complex formed by GO and a fluorophore (GOF) through static quenching can have its K_{as} value calculated as in a chemical interaction process, given by equation 5:

$$K_{as} = \frac{[GOF]^X}{[GO_f]^Y \times [F_f]^Z} \quad (5)$$

where $[GOF]^X$ represents the concentration of the non-fluorescent complex raised to its stoichiometric coefficient X, $[GO_f]^Y$ represents the concentration of free GO raised to its stoichiometric coefficient Y, and $[F_f]^Z$ represents the concentration of free fluorophore raised to its stoichiometric coefficient Z. The exact values of the

stoichiometric coefficients for a chemical interaction/reaction require a comprehensive laboratory study of its molar proportions, being determined empirically. Furthermore, even for purely theoretical calculations, defining the molar concentration of GO is a hindrance.

Thus, to enable the estimated calculation of K_{as}, it is proposed to replace the molar concentration of GO in equation 5 with the concentration of static quenching sites (sqs) (equation 6). The proposed definition of a static quenching site (sqs) is a specific region on the GO surface that interacts with a single molecule/ion of fluorophore, forming a single non-fluorescent complex, ensuring a 1:1 F:GOF ratio. The approximation of other fluorophore molecules to this site would be hindered by steric effects and repulsion interactions.

The size of this site varies depending on the characteristics of the system and can change according to the pH of the medium, net charge of the fluorophores, and distribution of functional groups on the quencher surface. The definition of this site encompasses any groups capable of interacting strongly with the fluorophore, whether through covalent bonding, electrostatic attraction, or as acceptors or donors of hydrogen bonding. Thus, regardless of the lateral size distribution pattern and functional groups of the GO sheets, the stoichiometry of the interaction will remain 1:1 for GO:F (equation 7). Another consideration is that as long as the quenching efficiency is not equal to 100% of the fluorophore emission, there will be no free static quenching sites of GO. Therefore, the term $[sqsGO_f]^1$ represents the limiting reagent of the formation reaction of the non-fluorescent complex and can be removed from equation 6 as it is completely consumed. As a result, equation 7 can be simplified to equation 8:

$$K_{as} = \frac{[sqsGOF]^V}{[sqsGO_f]^W \times [F_f]^Z} \quad (6)$$

$$K_{as} = \frac{[sqsGOF]^1}{[sqsGO_f]^1 \times [F_f]^1} \quad (7)$$

$$K_{as} = \frac{[sqsGOF]^1}{[F_f]^1} \quad (8)$$

Even though simplified, equation 8 is not capable of calculating the value of K_{as} using directly the fluorescence intensity values. Therefore, it is necessary to observe the mathematical behavior of the system in a particular case, where static quenching is zero or close to zero. The static and dynamic quenching mechanisms commonly occur simultaneously, with their relative contributions varying for each system. Thus, when the occurrence of static quenching mechanism in a system is not favored, there will be a negligible difference between the concentration of static quenching sites on the surface of GO before and after the quenching process. By substituting the description of K_{as} (equation 7) into the modified Stern-Volmer equation (equation 3), it can be rewritten as equation 9:

$$\log\left(\frac{F_0 - F_q}{F_q}\right) = \log\frac{[sqsGOF]^1}{[sqsGO_f]^1 \times [F_f]^1} + n \times \log[sqsGO_i] \quad (9)$$

Taking the antilog in equation 9, it is possible to obtain equation 10, which can be simplified into equation 11, since $[sqeGO_f]^1$ and $[sqeGO_i]^n$ are approximately equal:

$$\frac{F_0 - F_q}{F_q} = \frac{[sqsGOF]^1}{[sqsGO_f]^1 \times [F_f]^1} \times [sqsGO_i]^n \quad (10)$$

$$\frac{F_0 - F_q}{F_q} = \frac{[sqsGOF]^1}{[F_f]^1} \quad (11)$$

With equation 11, it is possible to calculate the ratio between the concentrations of sqsGOF and F_f using only the fluorescence intensities of the system before and after the addition of the quencher. By equating equations 11 to 8, it is therefore possible to calculate the association constant (K_{as}) for the formation of the non-fluorescent complex of the GO-fluorophore pair using only the fluorescence intensity values of the system (equation 12):

$$K_{as} = \frac{F_0 - F_q}{F_q} = \frac{[sqsGOF]^1}{[F_f]^1} \quad (12)$$

Since the value of the fluorescence intensity of the fluorophore in the absence of the quencher is represented by F_0, and in its presence by F_q, the fluorescence intensity given by subtracting F_q from F_0 precisely represents the amount of emission that did not occur after the formation of the non-fluorescent complex (sqsGOF).[1] On the other hand, the value of the fluorescence intensity given by F_q represents the amount of emission from the free fluorophores, that is, those that did not participate in the formation of the non-fluorescent complex. Therefore, by equating equations 11 to 8, both the physical-chemical and mathematical meanings are maintained.

Using this methodology, it is possible to calculate the values of K_{as} and, consequently, the values of ΔG_{as} for each concentration of GO used to form the GO-fluorophore (Table 1).

For concentrations of GO up to 15.62 μg mL^{-1}, the formation of the non-fluorescent complex GO-FS is unfavorable, indicating a predominance of the dynamic

Table 1. Variation of Gibbs free energy for the association of GO-fluorophore interaction (FS, MB, and NP), at concentrations of GO between 0.12 and 250 μg mL^{-1} and fluorophore concentrations of 100 and 10 nmol L^{-1}

GO / (μg mL^{-1})	ΔG_{as} / (J mol^{-1})					
	FS 100 nmol L^{-1}	FS 10 nmol L^{-1}	MB 100 nmol L^{-1}	MB 10 nmol L^{-1}	NP 100 nmol L^{-1}	NP 10 nmol L^{-1}
250	–2767.23	–2699.21	–2403.56	–623.80	337.42	341.81
125	–1976.67	–1576.28	–2143.50	–427.74	1331.70	1739.24
62.5	–1298.57	–826.06	–1798.92	297.88	1895.12	1718.80
31.25	–640.89	–188.40	–1716.43	400.72	2149.87	3056.08
15.62	229.53	551.95	–1542.69	964.90	2404.62	4289.66
7.81	617.99	1319.58	–1606.26	936.29	5001.86	5523.23
3.90	1006.45	1880.26	–1534.38	1885.01	3413.07	3337.28
1.95	1337.61	2503.42	–1605.56	2820.70	2556.83	4447.27
0.97	3980.79	3877.81	–1146.23	1478.77	3200.83	3664.69
0.48	2561.16	2788.06	–87.57	1366.48	3912.15	2882.10
0.24	3384.77	4414.71	1604.47	4211.65	3823.59	4592.96
0.12	4153.10	5169.01	2464.56	2545.60	2936.67	3961.71

ΔG_{as} is the variation of free energy of Gibbs for the association of non-fluorescent complex; GO: graphene oxide; FS: fluorescein sodium; MB: methylene blue; NP: naphthalene.

quenching mechanism of FS fluorescence emission. This result shows that even at this concentration of GO, there is still a predominance of repulsion forces between the net charges of FS (dianionic form) and GO at pH 7.4. With the increase in the concentration of GO, there is a gradual favoring of the formation of the non-fluorescent complex (static quenching mechanism). This result is attributed to the decrease in available space in the medium with the increase in GO concentration, forcing an approximation between GO and FS, and allowing the formation of hydrogen bonds between their oxygenated groups. By varying the concentration of FS from 10 to 100 nmol L^{-1}, little change in the described pattern was observed, with the static quenching mechanism starting to be favorable from 15.62 μg mL^{-1} of GO onwards. This result indicates that the concentration of FS has little influence on the formation of the non-fluorescent complex, as expected from a predominantly long-distance interaction (dynamic quenching). In a dynamic quenching process, the quenching efficiency is inversely proportional to the square of the distance between the quencher and fluorophore. Thus, increasing the concentration of one of the elements involved in quenching will only affect the efficiency of energy transfer if its area or volume occupies the available space in the medium.

In this case, the only element capable of exerting such influence would be GO (with an average area of 2.0×10^{-2} μm^2, whereas FS has only 7.85×10^{-7} μm^2). FS and its derivatives are typically used together with GO in the construction of biosensor systems through dynamic quenching mechanism.[11,58,59] In other cases, its adsorption on the surface of GO is described,[60] corroborating the result of dual quenching capacity in the GO-FS system, as observed in the present study.

In the GO-MB system, the concentration of 100 nmol L^{-1} of MB shows negative values of ΔG from low concentrations of GO (less than 0.49 μg mL^{-1}), indicating the predominance of the static mechanism in the quenching phenomenon of MB fluorescence emission caused by GO. This interaction occurs predominantly through electrostatic attraction between the opposing net charges of MB (cationic form) and GO at pH 7.4. In contrast, the increase in GO concentration gradually favors the formation of the non-fluorescent complex GO-MB. At low concentrations of GO, this is not observed, which can be explained by the statistically low probability of encounters in the medium, since their movements are governed by Brownian motion and convection due to minor changes in local temperature. Decreasing the MB concentration to 10 nmol L^{-1} significantly decreased the occurrence of the static quenching mechanism. This result aligns with expectations for a short-range interaction, characteristic of static quenching, as reducing either the GO or MB reagent significantly hinders the formation of the product (non-fluorescent GO-MB complex).

The high adsorption capacity of the MB dye onto the surface of GO has been extensively described in the literature.[51-54] Additionally, the work by Pahang *et al.*[54] also assessed the fluorescence quenching of MB emission by GO, suggesting the predominance of the static quenching mechanism. It is noteworthy that the authors found a K_{as} value of 0.04 for the GO-MB interaction using only the

Stern-Volmer curve. However, this K_{as} value would result in a ΔG value of 3.4 kJ mol^{-1}, indicating unfavorable static quenching. Applying the methodology proposed in the present study, the data presented by the authors generated ΔG values ranging from 383 to –436 J mol^{-1}, approximately, with increasing GO concentration.

Finally, for the GO-NP system, all calculated ΔG_{as} values were positive, showing no clear trend with the variation of the reagents. In other words, the formation of the non-fluorescent GO-NP complex was disfavored in any composition of the system. In NP, the absence of functional groups containing heteroatoms, capable of interacting more strongly with the quencher, restricts the quenching of NP emission by GO to moments of proximity between them, characterizing dynamic quenching. These results also corroborated with previous studies, where Wang *et al.*[61] demonstrated the low capacity of GO to adsorb naphthalene.

Since the ratio of [sqsGOF] to [sqsGO] is 1:1, the Stern-Volmer equation (equation 1) can be applied using the molar concentration of the static quenching sites of GO, and the graphs in Figure 2d can be re-plotted (Figure 3).

By using the values of [sqsGO] in the Stern-Volmer equation, it is possible to observe that the fluorophores FS and MB exhibit two distinct patterns as the concentration of GO increases. Initially, the relationship between F_0/Fq is linear with an invariant term close to 1, indicating a good fit to the Stern-Volmer curve and the predominance of a single type of quenching. Interestingly, beyond certain [sqsGO] values (44.68 for FS and 52.04 for MB), there is a deviation from the linearity of the curve, consistent with simultaneous static and dynamic quenching. These values correspond to the points in Table 1 where ΔG_{as} becomes negative (31.25 μg mL^{-1} for FS and 0.48 μg mL^{-1} for MB). Unlike Figure 1d, the replot accurately indicates the points where both static and dynamic quenching are favored. Another noteworthy point is that, although commonly associated with a deviation described by a quadratic curve, the deviation observed in Figure 3 is better described by the Michaelis-Menten model (equation 13).

$$y = \frac{ax}{b + x} \tag{13}$$

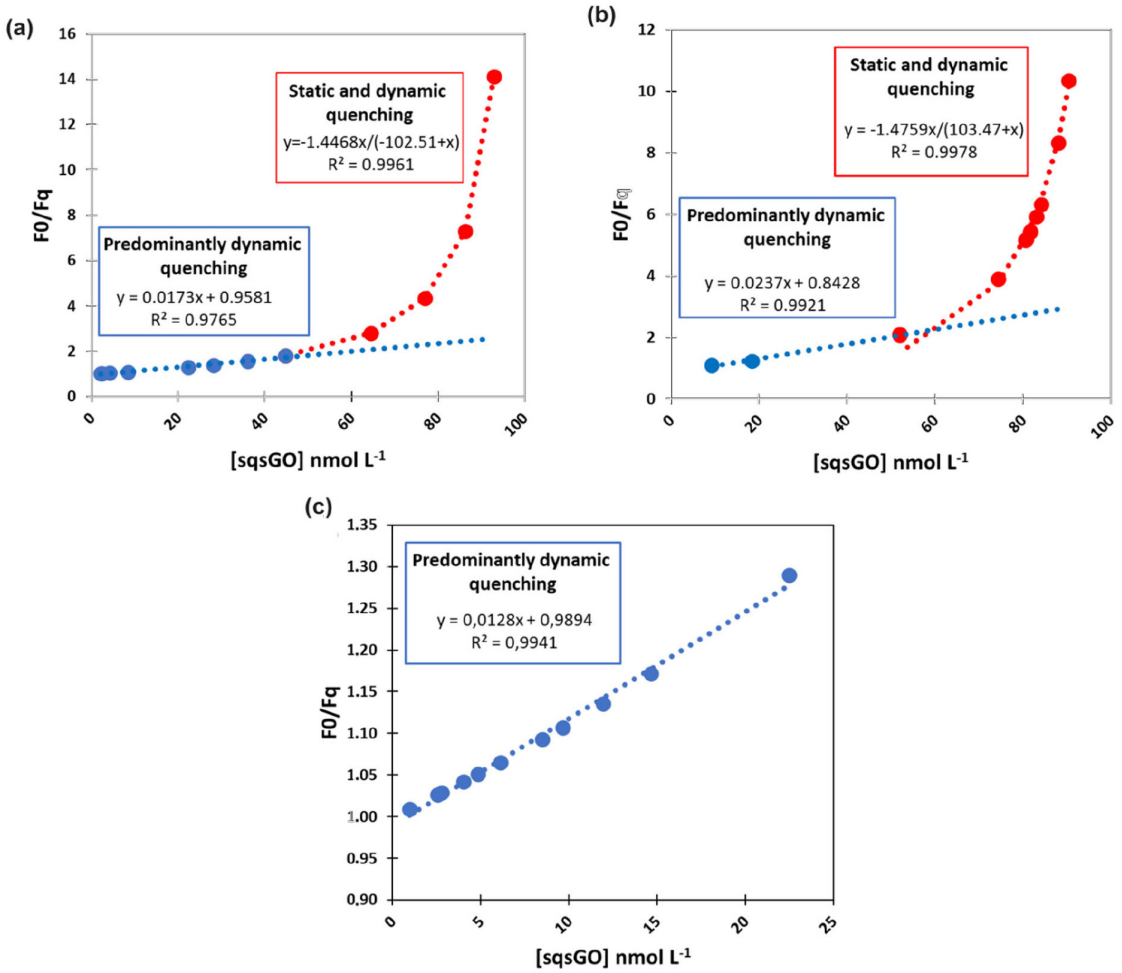

Figure 3. Sterm-Volmer plot in function of [sqsGO] for (a) fluorescein sodium (FS) (b) methylene blue (MB) and (c) naphthalene (NP) at 100 nmol L^{-1}.

The Michaelis-Menten mathematical model describes the kinetics of enzymes, particularly those exhibiting substrate saturation. This involves the formation of an enzyme-substrate complex, where enzymes have saturable active sites and substrates are in excess. Interestingly, static quenching interactions between graphene oxide (GO) and fluorophores also form complexes, with fluorophores in excess and GO potentially saturating active sites. Additionally, GO sheets are of similar lateral size scale to enzymes. Thus, the GO interaction pattern in forming non-fluorescent complexes more closely resembles enzyme-substrate interactions than atomic-scale interactions between two substances.

The methodology proposed in this study has limitations, since it is based on certain assumptions. Very recently, Genovese *et al.*[57] proposed the equations necessary to study the process of static quenching without any approximations. However, such methodology has limited applicability for dispersions containing a heterogeneous pattern in their physicochemical characteristics of size and functional groups, as mentioned earlier. Thus, the methodology proposed in this study becomes more suitable for performing approximate and point-to-point calculation of the association constant of these systems with heterogeneous characteristics, such as dispersions of nanomaterials like graphene and its derivatives.

Thus, a diagram (Figure 4) was proposed suggesting the interaction between GO and the fluorophores FS, MB, and NP, at concentrations below 31.25 μg mL^{-1} of GO.

In summary, in the GO-MB system (Figure 4a), the opposite net charges lead to electrostatic attraction between them, favoring the static fluorescence quenching mechanism. It is worth noting that, as observed in Table 1, at low concentrations of GO or MB, static quenching is disfavored due to the low collision rate between MB and GO in the medium. In the GO-NP system (Figure 4b), electrostatic interaction does not predominate due to the homogeneous distribution of electrostatic potential in the nonpolar NP molecule. Therefore, it is believed that NP emission quenching will predominantly be of the dynamic type during the probabilistic encounter between quencher and fluorophore in Brownian motion. Finally, in the GO-FS system (Figure 4c), electrostatic repulsion is expected, favoring dynamic fluorescence quenching at low concentrations of GO. However, as the GO concentration increases, the collision rate with sufficient energy to overcome such repulsion and favor hydrogen bonding interaction between GO and FS increases. It is also possible that FS adsorbs onto the surface of GO through π-π interactions. This can explain the favoring of static quenching of FS emission observed in Table 1 after 31.25 μg mL^{-1} of GO.

The interaction of a static quenching site of GO with the fluorophores FS, MB, and NP, as defined here, can

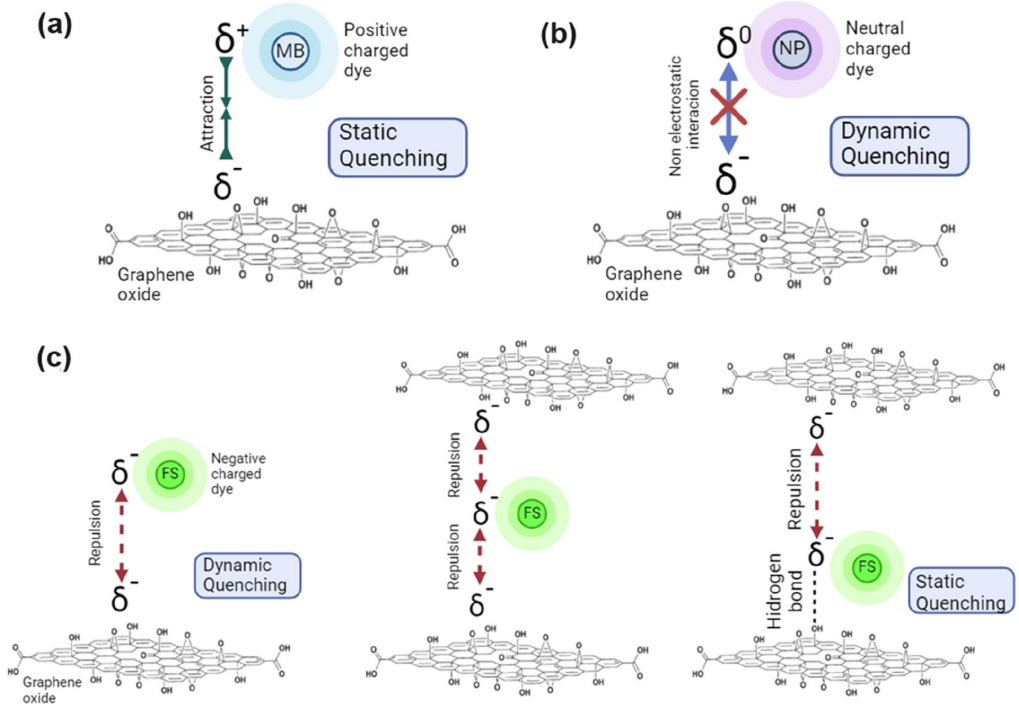

Figure 4. Proposed scheme for the interaction between GO (negative net charge) and the fluorophores (a) MB (positive net charge), (b) NP (neutral), and (c) FS (negative net charge). The GO model utilized was proposed by Lerf[45] and designed by Compton and Nguyen.[62] GO: graphene oxide; MB: methylene blue; NP: naphthalene; FS: fluorescein sodium.

also be analyzed by representing their chemical structures along with their respective molecular electrostatic potential (MEP) (Figure 5).

In Figure 5a, the heterogeneity of the electrostatic potential is observed on the surface of GO (represented here by the industrial GO molecule CID 163320950 from PubChem), with predominance of polar regions (negative net charge). Thus, repulsion of the predominant polar regions in the FS molecule (negative net charge) (Figure 5b) is predicted. On the other hand, MB (Figure 5c), having a concentrated polar MEP (and positive) mainly at one point, can easily interact with GO. It is also noted that on the represented surface of GO, there is more than one possible static quenching site for MB, which explains the rapid increase in MB emission quenching efficiency observed in Figure 2c. Lastly, in Figure 5d, it is observed that the oxygenated groups on the surface of GO may decrease the ability of NP to engage in π-π interactions with GO due to steric effects.

Applying this new mathematical approach to estimate K_{as} and ΔG_{as} of systems composed of GO as a fluorescence quencher and a charged fluorophore of interest is particularly significant in the field of optical sensors. The use of this new mathematical approach can assist in understanding the interaction between GO and the fluorophore, as well as in describing the quenching mechanism, determining the optimal concentration of GO or fluorophore to favor one mechanism over the other in the system, and ultimately ensuring the reproducibility of sensor construction and response signal.

Another application in the environmental field is the estimation of the stoichiometric ratio of GO concentration needed for use in the adsorption of pollutant dyes. Since static quenching is caused by an adsorption interaction, evaluating when it is more favorable can be useful to optimize the conditions for the adsorption of pollutant dyes in water by GO.

Conclusions

With some assumptions about the system behavior, the Stern-Volmer equation can be modified to be enable calculating the association constant (K_{as}) and the change in Gibbs free energy (ΔG_{as}) in systems composed of graphene oxide as a quencher and three fluorophores with distinct charges. The promotion of non-fluorescent complex formation with increasing graphene oxide (GO) concentration was observed in systems containing charged fluorophores, while the neutral fluorophore did not show strong enough interactions. The negatively charged fluorophore (fluorescein sodium) exhibited the greatest influence of its charge and the concentration of

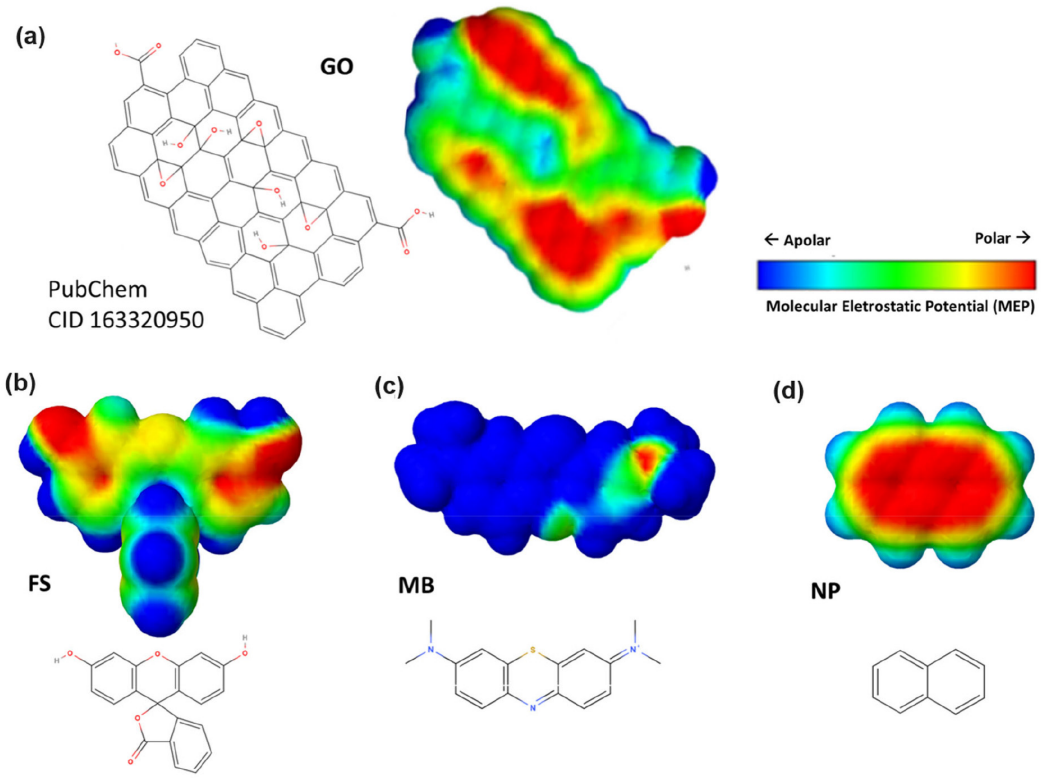

Figure 5. Schematic representation of the interaction of a static quenching site of (a) graphene oxide (GO) and the fluorophores (b) fluorescein sodium (FS), (c) methylene blue (MB) and (d) naphthalene (NP) visualized on a scale of molecular electrostatic potential (MEP).

GO on the fluorescence quenching mechanism, for which there is a range of GO concentrations that predominantly leads to repulsion between them and consequently favors dynamic quenching, and another range potentially leading to the formation of hydrogen bonds, resulting in the non-fluorescent complex responsible for the static quenching mechanism.

Experimental

Materials

Grounded expanded graphite was purchased from Nacional de Grafite Ltda. (Itapecerica, Brazil). Methylene blue (MB), fluorescein sodium (FS) and naphthalene (NP) were purchased from Sigma-Aldrich, Merck (St. Louis, USA). All other materials were of analytical grade and available commercially.

To prepare the 500 μmol L^{-1} FS solution, 18.8135 mg of analytical grade (purity of 98.5%) FS were weighed and dissolved in 100 mL of ultrapure water with manual stirring. To prepare 500 μmol L^{-1} MB solution, 15.993 mg of analytical grade (purity greater than 96%) MB were weighed and dissolved in 100 mL of ultrapure water. To prepare the 500 μmol L^{-1} NP solution, 6.4085 mg of analytical grade (purity of 99%) NP were weighed and mixed to 100 mL of ultrapure water. To dissolve the naphthalene in water, the mixture was kept in a sealed amber flask and stirred magnetically for 48 h. The resulting solution (FS, MB and NP), with a concentration of 500 μmol L^{-1}, was then diluted to 500 nmol L^{-1} by mixing 100 μL of the original solution with 99.9 mL of ultrapure water. Finally, a 50 nmol L^{-1} solution was prepared by diluting the 500 nmol L^{-1} solution 1:10 ratio with ultrapure water. The samples were stored in amber bottles and kept at 4 °C until the date of use.

Synthesis of graphite oxide (GrO) and graphene oxide (GO)

For the synthesis of GrO, the modified Hummer's method proposed by Marcano *et al*.[23] was employed. Briefly, in a reflux system immersed in an ice bath, a mixture of sulfuric acid and phosphoric acid (9:1) was added, followed by slow addition of 10 g of ground expanded graphite and 60 g of potassium permanganate. The system was kept at 50 °C for 12 h and then cooled to room temperature. Then, 800 g of deionized water ice were added, and the system was refrigerated for 12 h for phase separation. The decanted solution was reserved, and the supernatant was centrifuged (7000 g for 4 min) for material recovery. To the recovered and decanted material was added 250 mL of HCl 0.01 mol L^{-1}. The mixture was then centrifuged at 10,000 g for 4 min. The subsequent step involved successive washes (addition of solvent and centrifugation at 11,000 g for 10 min), alternating between deionized water and absolute ethanol until the supernatant was clear. The last wash used a 0.01 mol L^{-1} NaOH solution to neutralize the remaining acid. Upon reaching pH 9.8, the mixture was coagulated by adding 600 mL of diethyl ether and vacuum filtered (filter paper with a pore size of 0.4 μm). The GrO was vacuum-dried at 60 °C for 12 h.

The exfoliation of GrO into an aqueous dispersion of 500 mg mL^{-1} of GO was carried out using a probe ultrasound disperser (Sonics Vibra-Cell VCX750, USA), totaling 38 kJ of energy.

Instrumental analysis

GrO was characterized by X-ray diffractometry (DRX), potentiometric titration, attenuated total reflectance-Fourier transform infrared spectroscopy (ATR-FTIR), monochromatic X-ray photoelectron spectroscopy (XPS) and Raman spectroscopy. DRX was performed using an Ultima III equipment (Rigaku, Japan) with a Cu Kα radiation source. The analysis was conducted in the range of 4 to 90°, with a step size of 0.02° and a speed of 4° *per* min. Potentiometric titrations were carried out in a Tritano automatic titrator (Metrohm, Switzerland) with 0.02 mol L^{-1} NaOH and 0.001 mol L^{-1} HCl solutions. ATR-FTIR spectra were obtained with a LUMOS II FTIR microscope (Bruker, USA). The sample was deposited on Si/SiO_2 wafers and vacuum dried. XPS analyses were performed with a K-Alpha spectrometer (ThermoScientific, USA) with Al Kα (1486.6 eV) radiation. Raman spectra were obtained using the iHR550 equipment (Horiba, France) with argon laser (489 nm). The spectra were measured by 10 accumulations with an integration time of 20 s using a 10× objective.

GO was characterized by transmission electron microscopy (TEM), and atomic force microscopy (AFM). TEM images were acquired in a Tecnai G2-12 SpiritBiotwin 120 kV microscope (FEI, USA), and the dispersion was deposited onto a holey carbon TEM grid and vacuum dried. AFM images were acquired in an Asylum Research Cypher ES microscope (Oxford Instruments, United Kingdom). The samples were deposited on Si/SiO_2 wafers functionalized with 3-aminopropyltriethoxysilane (APTES) and dried with a jet of compressed nitrogen. The analysis of the AFM images was conducted using the particle analysis toolbox in ImageJ,[63] which determined the lateral dimensions of each flake.

Stationary fluorescence analyses were performed on an EnSpire spectrofluorometer (PerkinElmer, USA) with a

slit width of 10 nm, using a Brandplates-pureGrade white flat-bottom plate with 96 wells.

Effect of graphene oxide concentration in fluorescence quenching

In the assays, 55 µL of pH 7.4 phosphate buffered saline (PBS) buffer (1.44 g L^{-1} of Na_2HPO_4, 0.2 g L^{-1} of KCl and 0.24 g L^{-1} KH_2PO), 25 µL of GO (concentration between 250 and 0.12 µg mL^{-1}), and 20 µL of FS (100 and 10 nmol L^{-1}) were added to each well. The fluorescence emission intensity spectrum was read between 500 and 550 nm under excitation at 483 nm in 25 °C. For the quencher effects of GO analyses, the area under the FS emission curve was used. For the other fluorophores, the same concentrations of 100 and 10 nmol L^{-1} were maintained, and the stationary fluorescence emission spectra were obtained around their respective emission peaks in 25 °C, namely MB (λ_{exc} 640 nm and λ_{emis} 660 to 720 nm) and NP (λ_{exc} 280 nm and λ_{emis} 300 to 370 nm). At pH 7.4, the ionic forms of fluorophores are dianionic for FS and cationic for MB. NP do not have an ionic form and maintain a neutral net charge at neutral pH.

Three-dimensional modelling

Using data available on the PubChem platform, the three-dimensional model containing the molecular electrostatic potential (MEP) surface of each compound and GO was created on the MolView[64] platform with the assistance of Jmol.[65]

Acknowledgments

This work was supported by the Brazilian Nanocarbon Institute, Teranostic Nanomedicine, Translational Research in Oncology, 2D Networks of Minas Gerais, and the Brazilian agencies CAPES, CNPq, FAPEMIG and FINEP. The authors would like to thank the UFMG Microscopy Center team for the microscopy images.

Author Contributions

Danilo R. C. Ferreira was responsible for conceptualization, data curation, formal analysis, investigation, writing original draft; Tiago Serodre for data curation, writing (original draft, review and editing), investigation; Pedro L. Gastelois for data curation, writing (review and editing); Waldemar A. A. Macedo for investigation, writing (review and editing), funding acquisition; Estefânia M. N. Martins for formal analysis, writing (review and editing), investigation, funding acquisition, project administration; Clascídia A. Furtado for conceptualization, formal analysis, writing (original draft, review and editing), investigation, funding acquisition, project administration.

References

1. Lakowicz, J. R. In *Principles of Fluorescence Spectroscopy*; Lakowicz, J. R., ed.; Springer: Boston, USA, 2006, p. 277. [Crossref]
2. Eftink, M. R.; Ghiron, C. A.; *Anal. Biochem.* **1981**, *114*, 199. [Crossref]
3. Ma, C. Q.; Li, K. A.; Tong, S. Y.; *Anal. Chim. Acta* **1996**, *333*, 83. [Crossref]
4. Ren, S.; Giusti, M. M.; *Foods* **2021**, *10*, 310. [Crossref]
5. Shinitzky, M.; Rivnay, B.; *Biochemistry* **1977**, *16*, 982. [Crossref]
6. Fischkoff, S.; Vanderkooi, J. M.; *J. Gen. Physiol.* **1975**, *65*, 663. [Crossref]
7. Kim, J.; Cote, L. J.; Kim, F.; Huang, J.; *J. Am. Chem. Soc.* **2010**, *132*, 260. [Crossref]
8. Kong, Z.; Daab, M.; Yano, H.; Huang, H.; Breu, J.; Sasaki, T.; Nguyen, S. B. T.; Huang, J.; *Small Methods* **2020**, *4*, 2000036. [Crossref]
9. Moyon, N. S.; Mitra, S.; *J. Phys. Chem. B* **2011**, *115*, 10163. [Crossref]
10. Howerton, S. B.; Goodpaster, J. V.; McGuffin, V. L.; *Anal. Chim. Acta* **2002**, *459*, 61. [Crossref]
11. Shi, J.; Chan, C.; Pang, Y.; Ye, W.; Tian, F.; Lyu, J.; Zhang, Y.; Yang, M.; *Biosens. Bioelectron.* **2015**, *67*, 595. [Crossref]
12. Yang, D. M.; Fu, T. F.; Lin, C. S.; Chiu, T. Y.; Huang, C. C.; Huang, H. Y.; Chung, M. W.; Lin, Y. S.; Manurung, R. V.; Nguyen, P. N. N.; Chang, Y. F.; *Biosens. Bioelectron.* **2020**, *168*, 112571. [Crossref]
13. Zhang, Q.; Yin, B.; Huang, Y.; Gu, Y.; Yan, J.; Chen, J.; Li, C.; Zhang, Y.; Wong, S. H. D.; Yang, M.; *Biosens. Bioelectron.* **2023**, *230*, 115270. [Crossref]
14. Chen, J.; Zhang, Y.; Wang, X.; Li, F.; Wu, S.; Wang, W.; Zhou, N.; *Anal. Biochem.* **2024**, *688*, 115462. [Crossref]
15. Morales-Narváez, E.; Merkoçi, A.; *Adv. Mater.* **2019**, *31*, 1805043. [Crossref]
16. Xiao, X.; Zhang, Y.; Zhou, L.; Li, B.; Gu, L.; *Nanomaterials* **2022**, *12*, 2444. [Crossref]
17. Kuila, T.; Khanra, P.; Bose, S.; Kim, N. H.; Ku, B. C.; Moon, B.; Lee, J. H.; *Nanotechnology* **2011**, *22*, 305710. [Link] accessed in August 2024
18. Morales-Narváez, E.; Merkoçi, A.; *Adv. Mater.* **2012**, *24*, 3298. [Crossref]
19. Zhao, X. H.; Ma, Q. J.; Wu, X. X.; Zhu, X.; *Anal. Chim. Acta* **2012**, *727*, 67. [Crossref]
20. Li, W.; Jiang, T.; Pu, Y.; Jiao, X.; Tan, W.; Qin, S.; *Micro Nano Lett.* **2019**, *14*, 344. [Crossref]
21. Battisti, A.; Samal, S. K.; Puppi, D.; *Micromachines* **2023**, *14*, 1522. [Crossref]

22. Liu, Z.; Zhou, J.; Wang, X.; Zhao, J.; Zhao, P.; Ma, Y.; Zhang, S.; Huo, D.; Hou, C.; Ren, K.; *Spectrochimica Acta, Part A* **2024**, *305*, 123497. [Crossref]
23. Marcano, D. C.; Kosynkin, D. V.; Berlin, J. M.; Sinitskii, A.; Sun, Z.; Slesarev, A.; Alemany, L. B.; Lu, W.; Tour, J. M.; *ACS Nano* **2010**, *4*, 4806. [Crossref]
24. Stobinski, L.; Lesiak, B.; Malolepszy, A.; Mazurkiewicz, M.; Mierzwa, B.; Zemek, J.; Jiricek, P.; Bieloshapka, I.; *J. Electron Spectrosc. Relat. Phenom.* **2014**, *195*, 145. [Crossref]
25. Yan, H.; Tao, X.; Yang, Z.; Li, K.; Yang, H.; Li, A.; Cheng, R.; *J. Hazard. Mater.* **2014**, *268*, 191. [Crossref]
26. Saleem, H.; Haneef, M.; Abbasi, H. Y.; *Mater. Chem. Phys.* **2018**, *204*, 1. [Crossref]
27. Johra, F. T.; Lee, J. W.; Jung, W. G.; *J. Ind. Eng. Chem.* **2014**, *20*, 2883. [Crossref]
28. Cançado, L. G.; Jorio, A.; Pimenta, M. A.; *Phys. Rev. B* **2007**, *76*, 64304. [Crossref]
29. Jorio, A.; Saito, R.; Dresselhaus, G.; Dresselhaus, M. S.; *Raman Spectroscopy in Graphene Related Systems*, 1st ed.; John Wiley & Sons: New Jersey, USA, 2011.
30. Kaniyoor, A.; Ramaprabhu, S.; *AIP Adv.* **2012**, *2*, 32183. [Crossref]
31. Mehl, H.; Matos, C. F.; Neiva, E. G. C.; Domingues, S. H.; Zarbin, A. J. G.; *Quim. Nova* **2014**, *37*, 1639. [Crossref]
32. Beams, R.; Cançado, L. G.; Novotny, L.; *J. Phys.: Condens. Matter* **2015**, *27*, 83002. [Crossref]
33. King, A. A. K.; Davies, B. R.; Noorbehesht, N.; Newman, P.; Church, T. L.; Harris, A. T.; Razal, J. M.; Minett, A. I.; *Sci. Rep.* **2016**, *6*, 19491. [Crossref]
34. Anusuya, T.; Pathak, D. K.; Kumar, R.; Kumar, V.; *FlatChem* **2022**, *35*, 100422. [Crossref]
35. Kim, U. J.; Furtado, C. A.; Liu, X.; Chen, G.; Eklund, P. C.; *J. Am. Chem. Soc.* **2005**, *127*, 15437. [Crossref]
36. Surekha, G.; Krishnaiah, K. V.; Ravi, N.; Padma Suvarna, R.; *J. Phys. Conf. Ser.* **2020**, *1495*, 12012. [Crossref]
37. Botella, R.; Piñeiro-García, A.; Semetey, V.; Lefèvre, G.; *Mater. Lett.* **2022**, *320*, 132352. [Crossref]
38. Al-Gaashani, R.; Najjar, A.; Zakaria, Y.; Mansour, S.; Atieh, M. A.; *Ceram. Int.* **2019**, *45*, 14439. [Crossref]
39. Serodre, T.; Oliveira, N. A. P.; Miquita, D. R.; Ferreira, M. P.; Santos, A. P.; Resende, V. G.; Furtado, C. A.; *J. Braz. Chem. Soc.* **2019**, *30*, 2488. [Crossref]
40. Orth, E. S.; Ferreira, J. G. L.; Fonsaca, J. E. S.; Blaskievicz, S. F.; Domingues, S. H.; Dasgupta, A.; Terrones, M.; Zarbin, A. J. G.; *J. Colloid Interface Sci.* **2016**, *467*, 239. [Crossref]
41. Konkena, B.; Vasudevan, S.; *J. Phys. Chem. Lett.* **2012**, *3*, 867. [Crossref]
42. Shin, D. S.; Kim, H. G.; Ahn, H. S.; Jeong, H. Y.; Kim, Y. J.; Odkhuu, D.; Tsogbadrakh, N.; Lee, H. B. R.; Kim, B. H.; *RSC Adv.* **2017**, *7*, 13979. [Crossref]
43. Huang, Y.; Wu, J.; Hwang, K. C.; *Phys. Rev. B* **2006**, *74*, 245413. [Crossref]
44. Zhang, S.; Zhu, L.; Song, H.; Chen, X.; Wu, B.; Zhou, J.; Wang, F.; *J. Mater. Chem.* **2012**, *22*, 22150. [Crossref]
45. Lerf, A.; He, H.; Forster, M.; Klinowski, J.; *J. Phys. Chem. B* **1998**, *102*, 4477. [Crossref]
46. Cai, W.; Piner, R. D.; Stadermann, F. J.; Park, S.; Shaibat, M. A.; Ishii, Y.; Yang, D.; Velamakanni, A.; Sung, J. A.; Stoller, M.; An, J.; Chen, D.; Ruoff, R. S.; *Science* **2008**, *321*, 1162369. [Crossref]
47. Dimiev, A. M.; Polson, T. A.; *Carbon* **2015**, *93*, 544. [Crossref]
48. Motevalli, B.; Parker, A. J.; Sun, B.; Barnard, A. S.; *Nano Futures* **2019**, *3*, 45001. [Crossref]
49. Qiao, Q.; Liu, C.; Gao, W.; Huang, L.; *Carbon* **2019**, *143*, 566. [Crossref]
50. Van De Weert, M.; *J. Fluoresc.* **2010**, *20*, 625. [Crossref]
51. Liu, Y.; Liu, C. Y.; Liu, Y.; *Appl. Surf. Sci.* **2011**, *257*, 5513. [Crossref]
52. Wang, Q.; Sun, H.; Peng, T.; Yue, H.; *Huagong Xuebao (Chin. Ed.)* **2017**, *68*, 1712. [Crossref]
53. Srisantitham, S.; Sukwattanasinitt, M.; Unarunotai, S.; *Colloids Surf., A* **2018**, *550*, 123. [Crossref]
54. Pahang, F.; Parvin, P.; Bavali, A.; *Spectrochim. Acta, Part A* **2020**, *229*, 117888. [Crossref]
55. Barbero, N.; Barni, E.; Barolo, C.; Quagliotto, P.; Viscardi, G.; Napione, L.; Pavan, S.; Bussolino, F.; *Dyes Pigm.* **2009**, *80*, 307. [Crossref]
56. Wei, X. L.; Xiao, J. B.; Wang, Y.; Bai, Y.; *Spectrochim. Acta, Part A* **2010**, *75*, 299. [Crossref]
57. Genovese, D.; Cingolani, M.; Rampazzo, E.; Prodi, L.; Zaccheroni, N.; *Chem. Soc. Rev.* **2021**, *50*, 8414. [Crossref]
58. Cao, L.; Cheng, L.; Zhang, Z.; Wang, Y.; Zhang, X.; Chen, H.; Liu, B.; Zhang, S.; Kong, J.; *Lab-on-a-Chip* **2012**, *12*, 4864. [Crossref]
59. Ratajczak, K.; Stobiecka, M.; *J. Phys. Chem. B* **2017**, *121*, 6822. [Crossref]
60. Sari, M. M.; *Mater. Chem. Phys.* **2013**, *138*, 843. [Crossref]
61. Wang, J.; Chen, Z.; Chen, B.; *Environ. Sci. Technol.* **2014**, *48*, 4817. [Crossref]
62. Compton, O. C.; Nguyen, S. T.; *Small* **2010**, *6*, 711. [Crossref]
63. Rasband, W.; *ImageJ*, 2.0.0-rc-3; National Institutes of Health, USA, 2014.
64. Bergwerf, H.; *MolView*, v. 2.4; Bergwerf Labs Molview, Netherlands, 2012.
65. Gezelter, D.; *Jmol*, 16.1.59; University of Minnesota, USA, 2001.

Submitted: March 7, 2024
Published online: August 16, 2024